International Journal Of Engineering Research And Development
e- ISSN: 2278-067X, p-ISSN: 2278-800X, www.ijerd.com
Volume 17, Issue 4 (Jul. – Aug. 2021), PP. 51-62

Synthesis of a printed loop rectenna using metamaterials for effective RF energy harvesting

Christos Mourtzios[1] Katherine Siakavara[2]
[1,2]*Aristotle University of Thessaloniki*
School of Physics
Radiocommunications Laboratory
54124 Thessaloniki, Greece
Corresponding Author: Christos Mourtzios

ABSTRACT-*Radio-frequency (RF) energy harvesting (RFEH) has gained significant scientific attention as an efficient and promising method of enabling self-sustainable wireless sensors and networks. Metamaterial-enabled structures have been widely deployed to enhance the performance of a plethora of RF devices, especially in the microwave frequency regime. In this paper, a novel approach is presented on designing a low profile and compact rectenna (antenna and rectifier) employing a printed loop antenna integrated with a uniform Electromagnetic Band-Gap (EBG) structure operating at the 940MHz frequency regime. The presented analytical results proved that the proposed hybrid rectenna is superior to a respective rectenna without the EBG arrangement. Simulated voltage values (Voc) at the open circuited terminals of the printed loop reached a maximum of 0.96V/m for impinging circularly polarized (CP) waves of 1V/m electric field intensity. A Matching Network (MN) designed at 940MHz was connected between the antenna and the rectifier yields, at the output of the rectifier, DC voltage reaching to 0.42V and power, available at its input, reaching 26.6μW for perpendicularly incident waves. The overall performance of the proposed rectenna was estimated via statistical analysis of DC voltages and power values received, over frequencies around 940MHz and for multiple directions of arrival (DoAs) of incoming waves.*
Keywords - rectenna, Electromagnetic Band-Gap antennas, printed loop antennas, wireless energy harvesting, metamaterials

---

Date of Submission: 29-06-2021 Date of Acceptance: 13-07-2021

I. INTRODUCTION

'Green' and self-sustainable operation are fundamental attributes of emergent low-power technologies. Next generation wireless systems are designed and envisioned on a basis of a fully sustainable society, enabled by real time and seamless green connectivity. Meanwhile, artificial intelligence (AI), backscatter and visible light communications, edge computing and metamaterials will undoubtedly promote low energy/emission deployments (Liu,et al., 2019; Lopez, et al., 2019). The rise of Internet of Everything (IoE) introduces a world where billions of objects utilize autonomous and wireless embedded sensors connected over public or private networks using standard and/or proprietary telecommunication protocols. Retaining this massive number of standalone and energy-constrained sensors always-on, is still a challenging problem for the research community. Given that a plethora of sensors is installed in remote and possibly hazardous locations, renders battery maintenance even more challenging.

Energy Harvesting (EH) from various energy sources, seems to be an attractive candidate to effectively recharge batteries or power-up electronics wirelessly, avoiding replacement and eliminating human intervention (Divakaran, et al., 2019) even in scenarios where access is limited (bridges, chemical plants, airplanes), leveraging the ubiquitous energy sources. EH applications are mainly classified into ambient EH, collecting energy from resources that are already available in the environment, while dedicated EH relies on energy transmissions from dedicated energy sources to EH devices (Kim, et al., 2014). Numerous renewable ambient energy sources are omnipresent in nature (solar (Nguyen, et al., 2020), thermal (Hou, et al., 2018), piezoelectric (Mouapi, et al., 2015), microbial fuel cells (Yala-Ruiz, et al., 2019), acoustic energy (Awal, et al., 2016) and hybrid (Zhang, et al.,2019) which have been reported to successfully power electronic systems or sensors. Among them, Wireless Energy Harvesting (WEH) from Radio Frequency (RF) sources (Sandhya Lakshmi, 2015)has attracted significant attention due to the prevalence of electromagnetic (EM) energy from the ever-increasing RF sources such as Radio, cellular, satellite, TV and WiFi due the rapid expansion of Telecommunications and broadcasting deployments.

A WEH power system can capture and convert surrounding EM energy to usable DC voltage. Its fundamental compartments are an antenna unit, a rectifier circuit, usually a matching network between them, and a DC power storage unit, comprising a classical rectenna (Figure 1). The antenna senses and captures the available RF energy and the rectifier unit, then, converts it into DC signal. The matching network is utilized between the filter and rectifier circuit for optimal power transfer.

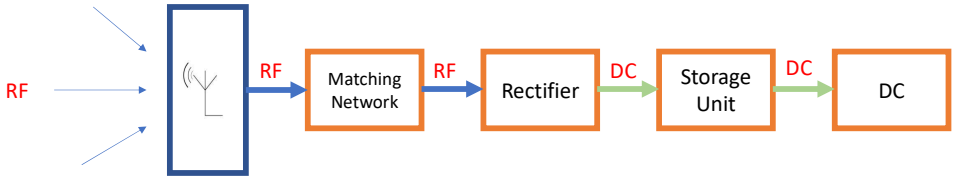

Figure 1: Typical rectenna system

Ambient RF energy has been reported to have an energy density of 0.2nW/cm^2-12nW/cm^2 which is classified low compared to other sources (Pinuela, et al., 2013). However, increased amounts of harvested RF power can be collected by deploying effective antenna designs. The antenna consists the front-end unit of a rectenna and its design is of prime importance, since it is responsible for the total input power inserted to the rectifying circuit, later to be processed by the following rectenna sub-systems.

There is a lot of speculation in international literature regarding different antenna types utilized in modern rectenna systems. An antenna design should exhibit wide operating frequency range, increased gain, omnidirectional radiation pattern and low-profile. The efficiency of the rectenna is a key metric related directly to the efficiency of the antenna and the rectifier circuit. The performance of the rectenna usually relies on the harvesting ability of the antenna and the power conversion efficiency (PCE) of the rectifier circuit. The PCE is defined as the ratio of the output DC power to the input RF power to the rectifier circuit.

In reported research, researchers have proposed various antenna types like monopole (Hong, et al., 2010), dipole (Zhu, et al., 2021), Yagi-Uda (Egashira, et al., 2020), inverted-F (Shen, et al., 2019), spiral (Khosht, et al., 1016), log-periodic (Song, et al., 2016), microstrip (Wang, et al., 2020), arrays (Assimonis, et al., 2018) used for RF energy harvesting applications demonstrating improved performance. Printed antennas are extensively deployed in modern microwave devices (Su, et al., 2011; Kang, et al., 2020) due to their inherent properties such as low-profile, light weight, ease of fabrication, low production cost and ease of incorporation with printed microwave structures.

In (Chen, et al., 2009) a low-cost meander loop rectifying antenna (rectenna) was presented designed at the frequency region 900-950MHz (Radio Frequency Identification Device, RFID band) achieving a maximum gain of 4.22 dBi and a radiation efficiency of 97% at 925 MHz. Authors in (Zeng, et al., 2017) presented a compact printed fractal loop rectenna for RF energy harvesting at GSM1800 frequency band employing a novel in-loop ground plane impedance matching. Measured results reported an efficiency of 61% and an output DC voltage of 1.8 V for a power density of 10μW/cm^2 at 1.8GHz, capable of powering up a battery-less LCD watch at a distance of 10m from the cell tower. A fractal geometry was introduced in (Shi, et al., 2018), the rectenna was designed to harvest WiFi RF energy utilizing a single stub matching network to achieve high conversion efficiency of up to 52% at 2.45GHz while researchers in (Huang, et al., 2020) designed a dual-band microstrip circular loop rectenna with measured results showing a maximum microwave-direct current (mw-dc) conversion efficiencies of 67.7% and 57.03% at 2.45 GHz and 5.8 GHz respectively. In (Rivière, et al., 2020) a coplanar waveguide (CPW) fed circular slot loop antenna is reported, matched to the standard 50Ω impedance by two stubs and fabricated on Arlon AD1000 substrate, (ε_r=10.35) achieving a simulated efficiency of 10% at-20dBm. In (Jianwei, et al., 2020) a compact and high-efficiency loop rectenna for wireless sensor applications at 2.45 GHz was reported. Experimental results showed peak microwave-to-dc conversion efficiency of 74% for an input power of 18dBm. The dimensions of rectenna were $30 \times 30 \times 1$ mm^3 weighting 0.58g providing a practical charging solution for wireless sensors.

Recently, new technologies have been employed for designing novel and efficient antenna systems. Metamaterials are engineered composites, widely integrated in microwave systems with intent to improve their overall performance. Several papers have reported rectennas exhibiting improved characteristics when integrated with metamaterial structures. In (Rashmi, et al., 2021), a wideband rectenna is proposed using a DGS (Defected Ground Structure) structure operating from 1.975 to 4.744 GHz with a single radiation patch. The peak conversion efficiency reported, was 88.58% at 0 dBm, 34.70% at 10 dBm, and 53.52% at 20 dBm under a load resistance of 100KΩ. In (Lee, et al., 2020) the authors presented a metamaterial-enabled dual-function loop antenna for wireless power transfer and wireless communication which operates at 6.78 MHz and 2.4 GHz

achieving a Wireless Power Transfer (WPT) efficiency improvement of 28.07 % and an antenna gain improvement of 1.89 dB compared to a respective structure without a metamaterial slab.

One of the most popular sub-genre of metamaterial media is the class of Electromagnetic Bandgap (EBG) structures. EBGs can be integrated with various antenna designs (Peddakrishna, et al., 2017) improving their radiation characteristics (Mourtzios, et al., 2014). Their attributes of surface wave elimination and the fact that they introduce zero reflection phase at the resonant frequency, renders them attractive for modern antenna and rectenna designs.

The present work concerns the synthesis of a rectenna system, employing a simple loop antenna printed on an EBG structure. The concept behind the proposed rectenna, lies on the exploitation of the EBG's attribute of exhibiting, at resonance, high levels of electromagnetic field intensity across the sides of its patches. The appropriate placement of a loop or loops in these areas of high field intensity, would cause the induction of high electromotive force and current in the loop which in turn would be guided to a rectifier for DC conversion. Therefore, the hybrid structure, loop and the EBG, would operate as an effective RF harvester. The whole system, antenna, matching network and rectifier was designed for RF energy scavenging within the band of 920MHz- 960MHz used usually for the downlink of mobile GSM900. The rectenna should bear the following attributes: low profile, improved radiation performance and sufficient power and V_{DC} at the rectifier. Moreover, as the rectenna is dedicated to collect RF power from waves propagating in a dense urban environment, rich in multipath phenomena, where the Directions of Arrival (DoAs) of the impinging waves are arbitrary, a large number of cases was considered and the performance of the rectenna was assessed via statistical processing of the respective results

In Section 2 the concept and theoretical analysis of EBGs are described, in Section 3 the methodology applied for the synthesis of the rectenna and the required calculation steps are presented, while Section 4 reports simulation results and elaboration on them. Section V reports the conclusions drawn.

II. THEORETICAL ANALYSIS OF EBG STRUCTURES

Electromagnetic band gap (EBG) designs consist of periodical geometric arrangements of dielectric materials and conductors that can allow or confine electromagnetic wave propagation within certain frequency regimes. Figure 2a presents a typical 'Mushroom' type EBG as reported at the seminal work of Sievenpiper,et al., 1999. It is a two-dimensional periodic array of identical equally spaced metallic patches attached on one side of a dielectric layer. The other side of the layer is coated with a very thin metallic layer used as ground. Thin metallic viases, embedded in the dielectric layer, connect conductively the patches to the ground metallic sheet. A very large number of hybrid 'antenna-EBG' designs have been proposed in the literature, as radiators exhibiting increased gain (Wu, et al., 2020) and frequency bandwidth (Zhang, et al., 2020) compared to typical antenna designs, side lobe (Abdulhameed, et al., 2020) and backward radiation reduction (Abdulhameed, et al., 2019) and Specific Absorption Rate (SAR) reduction (Imran, et al., 2021). In all cases they exploit one or more of the basic attributes of EBGs: a) their ability to suppress the surface waves and b) their inherent reflection properties. It is widely known that a perfect electric conductor (PEC) inserts 180° reflection phase to a normally incident plane wave, whereas a perfect magnetic conductor (PMC), which does not exist naturally, introduces 0° reflection phase. In contrast, an EBG lattice exhibits a PMC-like electromagnetic behavior, as its reflection coefficient phase varies continuously from 180° to -180°, through 0° at the surface's resonant frequency (Kildal, et al., 2015). This attribute guarantees in-phase image currents with respect to the antenna's currents and allows for low-profile antenna designs, as opposed to the case where an antenna is placed in front of a PEC reflector where the antenna-PEC distance should be λ/4 to counterbalance the 180° reflection phase caused by PEC.

Given that the periodicity of the EBG structures is relatively small compared to the wavelength of operation, the EBG structure can approximately be analyzed as an effective medium. The lattice interacts with impinging electromagnetic waves, currents are induced in the top metal patches and as they are interrupted by the gaps among the patches, charges are built up on the sides of adjacent patches and their presence ~~of which~~ results in a voltage difference. The whole mechanism can be equivalently described by a capacitance expressed by $C=\frac{W\,\varepsilon o(1+\varepsilon r)}{\pi}\cosh^{-1}(\frac{W+g}{g})$ where 'W' is the side length of the patch, 'g' is the distance between the patches, 'h' is the thickness of the substrate, 'r' is the radius of the pins, ε_0 is the permittivity of free space and ε_r is the substrate's permittivity. In parallel, the loop current circulating around the pins, the patches and the ground (Figure 2b) can be electrically represented by an inductance L calculated as L=μh, where μ is the permeability at free space. Therefore, the EBG's surface's impedance is equal to $Z=\frac{j\omega L}{1-\omega^2 LC}$, appearing a parallel resonance at the frequency $\omega_0=1/\sqrt{LC}$. Below resonance, the surface is inductive meanwhile above resonance, the surface is capacitive, while near ω_0, the surface impedance becomes high, prohibiting surface wave propagation across it.

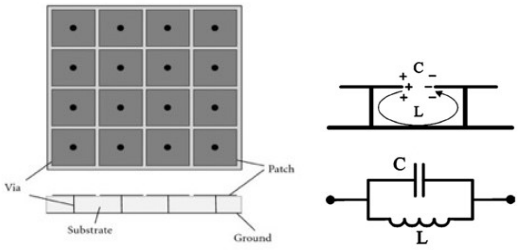

(a) (b)

Figure 2: a) Profile and panoramic view of a mushroom-like EBG lattice b) EBG equivalent circuit (Azarbar1and, et al., 2011)

The proposed rectenna system introduces a one-dimensional EBG array incorporated with a printed loop antenna. In this case, the EBG has not been used, as widely reported in literature, as a reflector or as a medium for suppressing surface waves. The novelty lies on leveraging the EBG's attribute of resonance and consequently the development of high field intensities at this resonance, as elaborated in the following section.

III. SYNTHESIS OF RECTENNA AND CALCULATION STEPS

In the present work, the reasonable assumption that EBG structures can enhance the performance of a printed loop rectenna was verified. The hybrid and low-profile rectenna was designed to collect effectively RF power from the regime of 920MHz-960MHz and from a wide range of DoAs to simulate conditions in a real urban environment rich in multipath phenomena. As discussed previously, a rectenna system consists of two fundamental units: the antenna, the rectifier and, if necessary, a matching network which is connected between them to ensure optimal power transfer from the antenna to the rectifier. The antenna synthesis is of main importance since this unit is responsible for collecting ambient EM energy to be processed by the rectifier. Therefore, the total output power and DC voltage at the rectifier are directly related to the initial EM energy collected by the antenna unit. The concept behind the proposed design is that the loop antenna will pump RF power from the electromagnetic field evolved under the patches, when the EBG structure is excited from the waves impinging on it at its frequency of resonance. So, the antenna is expected to direct more EM energy to the rectifier originating both, from the waves directly incident on the loop but additionally from the EBG's resonance. A criterion for the ascertainment of this expectation and for the, quantitatively, efficient performance of the antenna, is the voltage values, V_{oc}, induced at the loop's open circuited terminals when the structure operates as a receiver.

In order to validate the structure's resonance and define the antenna's location, simulation results of the surface currents were drawn. Figures 3(a),(b),(c) present the simulated magnetic fields at 920MHz, 940MHz and 960MHz respectively across the structure when plane waves imping on it, without the presence of the printed loop. Therefore the EBG is treated as a standalone passive receiving element at resonance. Maximum values of magnetic field intensity are observed at the edges of the central patches. The maximization of the magnetic field guarantees the maximization of the magnetic flux through the surface of the loop which in turn will induce high electromotive force and current at the loop when it will be positioned on the EBG. As a conclusion, this result is an indicator on where, approximately, the loop antenna should be placed in order to leverage the resonance phenomenon and achieve maximum Voc at 940MHz. Having identified the spots where the magnetic field maximizes, the loop antenna was added on top of the EBG unit in order to assess its ability to gather ambient EM energy. It was found that the areas of maximum magnetic field values appear around the middle of the entire EBG's length, namely at the two central patches. A necessary condition for this maximum to develop, is the presence of all six EBG patches. This performance, also, provides the ability to place more than one loops on the structure, selecting for each one an area of maximum. However, further research should take place, via simulations in presence of the loops, in order to redefine the structural parameters of the EBG since their presence affect the performance and the electromagnetic behavior of the entire structure.

The proposed rectenna system consists of the EBG structure, a printed loop antenna on top of it and the respective matching network. The EBG unit utilities six (6) identical and equi-spaced metallic patches connected to a copper ground through metallic thin pins (vias). The metallic lattice (patches and pins) is incorporated in a substrate dielectric layer of constant ε_r and thickness h. Another dielectric layer covers the whole structure having constant ε_{rc} and thickness h_c. The loop antenna is attached on top of the cover substrate ε_{rc}, above the third patch as depicted in Figure 4a. The exact position of the loop antenna and its dimensions were precisely tuned to maximize V_{oc} at its open circuited terminals when it operates as a plain wave receiver.

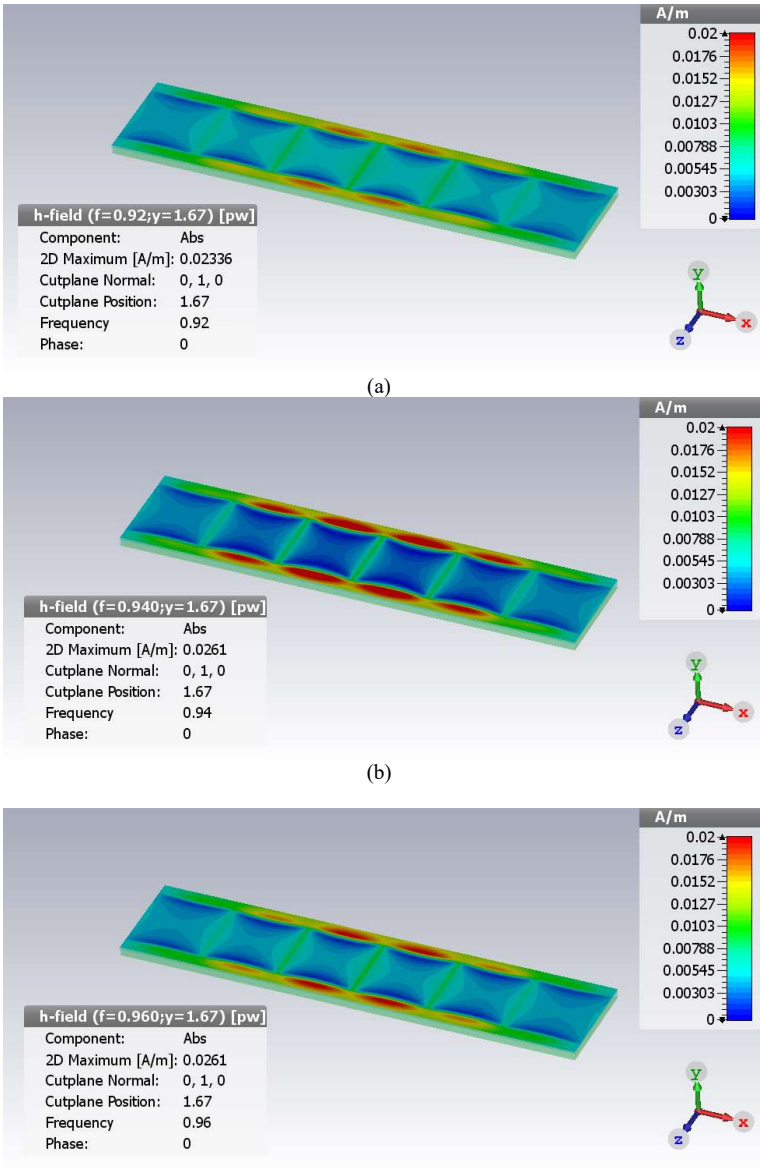

Figure 3: Surface plots of magnetic field intensity along the EBG structure (without the loop antenna and the rectifier circuit) when incident waves are imping perpendicularly on its surface at a) 920MHz b) 940MHz and c) 960MHz

The rectenna's structural parameters and their values are listed in Table 1 and constitute the proper combination in order to achieve maximum Voc at 940MHz. Their values were finalized via iterative modification of the initial structural values via simulations.

Table 1: Structural parameters and their values of the proposed loop-EBG antenna

Number of patches	**ε_r**	**ε_{rc}**	**h [mm]**	**h_c [mm]**	**Copper ground, patch and loop thickness [mm]**	**W1 (Side length of the patches) [mm]**	**g (distance between patches [mm]**	**Total size [mm]**
6	3.75	3.75	4.87	1.6	0.07	53	1	(L) 325 (W)73 (H) 6.6
Loop [mm]	L_{lp}=53.5	w_{lp}=10	d_{lp}=2					

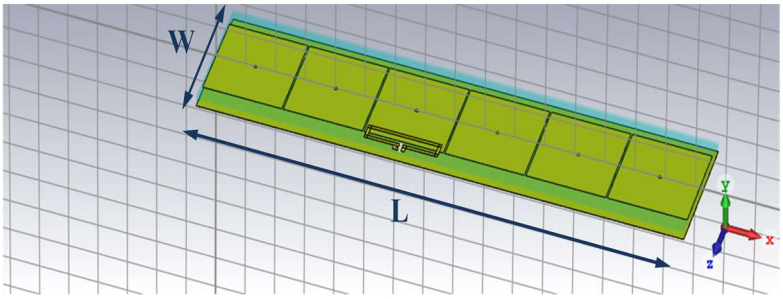

(a)

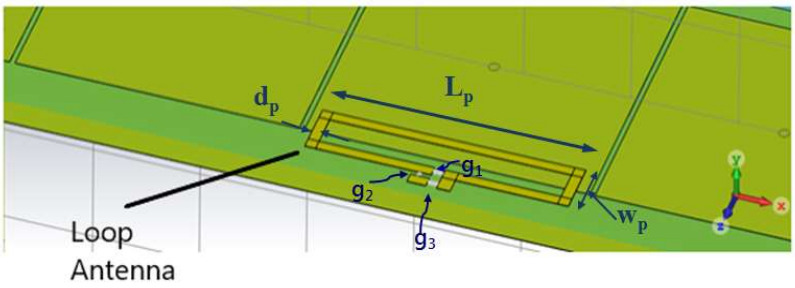

(b)

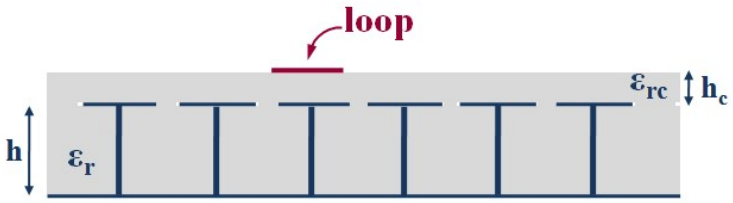

(c)

Figure 4: Layout of the hybrid EBG rectenna consisting of six (6) patches, the printed loop antenna and the rectifier circuitry a) top view b) the printed loop antenna and the locations at which the matching network components were connected c) profile view of the rectenna

The next step for the rectenna design, was the configuration of the rectifier circuit. A full wave rectifier was chosen with a 'smoothing', RC, circuit connected at its output. Based on microwave theory, when a rectenna's antenna operates as a receiver, it is equivalent to a voltage source, Voc, for the load at which it transfers the EM power collected from the environment. The Schottky diode HSMS-285C (Avago Technologies, 2020) was chosen for the implementation of the four-diode rectifier. Its equivalent circuit consists of a resistor of 3240 Ω in parallel with a capacitance of C=0.88pF. The necessary smoothing circuitry for the elimination of AC ripples is realized with capacitance C_o=1nF and resistance R_o=10 KΩ. These values ensure very low mean value of ripple, r, (less than 0.01%) of V_{DC}, given by formula $r = 1/(4\sqrt{3} f R_0 C_0)$. With intend to obtain maximum power transfer from the antenna to the rectifier, a Matching Network has to be connected between them. The MN ensures the conjugate matching between the input impedance of the antenna, $\dot{Z}_{in}$ (Figure 5), and the impedance of the rectifier, $\dot{Z}_{rec}$. The synthesis of MN was made by the respective microwave theory (Pozar, 2012). This theory concerns the matching between a resistive load and the impedance of a complex load. However, the input impedance of the antenna is not a resistive, so to overcome this problem we could connect a reactive load jX_A at the terminals of the antenna. The value of X_A was calculated in order to the parallel combination of $\dot{Z}_{in}$ and jX_P, termed as $\dot{Z}_{AB}$, to be an impedance having only real part at 940MHz. It was calculated that X_A has to be $X_A = 4.5 \cdot 10^3 Ohms$ and can be realized by an inductor $L_A = 763.7nH$. The entire equivalent circuitry is shown in Figure 5. After the connection of X_A, the MN elements were calculated with intend the resistive impedance $\dot{Z}_{AB} = 9.72 \cdot 10^3 Ohms$ to be matched to the $\dot{Z}_{rec}$. The MN's element values shown in Figure 5 were calculated to C_{MN}=1.96pF and L_{MN}=79.9nH for matching at 940MHz. In practice, and also in simulations, as the inductors L_A and L_{MN} are connected in parallel, they can be replaced by one microwave chip inductor (AVX-Advanced Electronic Components, 2020; Johanson Technology, 2020) of $L_{A\text{-}MN}$=68nH (commercial value). As C_{MN} could also be used a microwave chip capacitor

of *2pF* (AVX-Advanced Electronic Components, 2020; Johanson Technology, 2020). Both, in practice and in simulations, $L_{A\text{-}MN}$ is connected at the gap g_1 and C_{MN} at the gap g_2 shown in Figure 4b. The rectifier is connected to gap g_3.

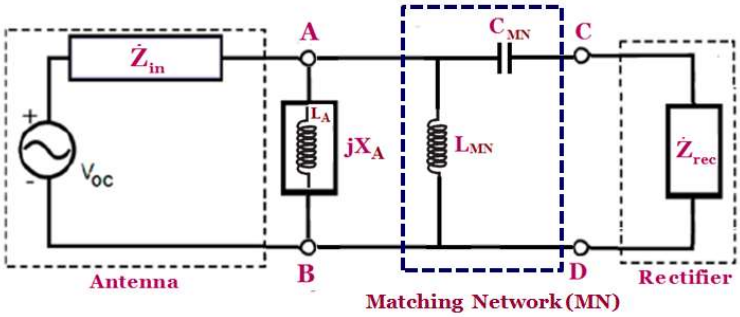

Figure 5: The antenna equivalent circuit connected to the rectifier via the matching network

Having defined the MN's values, P_{inrec} and V_{DC} were simulated. The available power at the rectifier's input, P_{inrec}, is given by formula:

$$P_{inrec} = Re(\dot{V}_{inrec} \cdot \dot{I}^*_{inrec}) \quad (2)$$

while

$$V_{DC} = \left|\dot{V}_{inrec}\right| / (1 + r\sqrt{3}) \quad (3)$$

where V_{inrec} is the voltage at the rectifier's input.

As it was previously mentioned the EBG structure was finely designed to resonate at 940MHz thus, resulting in maximum values of V_{oc} at this frequency. The quantities V_{inrec}, P_{inrec} and V_{DC} are directly proportional to the level of power of the impinging waves, their DoAs and the frequency. In practice all of these three parameters are impressed on V_{oc}. Consequently, in order to approach the problem more realistically and simulate real conditions, incoming waves from multiple DoAs and frequencies were taken into account treating the hybrid antenna as a receiving passive element and calculating via simulations the V_{oc} values. Then, using the received V_{oc} values and the solution process, concerning the aforementioned circuitry, P_{inrec} and V_{DC} values were calculated.

IV. RESULTS AND DISCUSSION

As described previously, the EBG system was designed to operate at 940MHz. Figure 6 depicts simulated V_{oc} versus frequency, for incident waves of different DoAs, measured at the loop antenna's open circuited terminals treating it as a passive receiving element. Maximum V_{oc} value was observed at 940MHz reaching 0.97V/m for perpendicularly ($\varphi=90^0$, $\theta=90^0$) impinging waves of field intensity 1V/m. Respective V_{oc} results for an identical structure using only the dielectric layers but without the EBG (metallic patches and pins) are also presented in Figure 6 to prove the necessity and superiority of the EBG enabled structure. For that case, maximum V_{oc} equal to 0.22V/m was obtained, which is five times less than the EBG-enabled proposed antenna. This result validates that the EBG is responsible for the increased V_{oc} levels due to the magnetic fields induced at the EBG at resonance. It is worth noting that V_{oc} values for oblique values of incidence, barely fall under 0.7V which implies immunity regarding DoA angles, and the fact that besides 940MHz, a second lower Voc peak at 1GHz appears which allows for energy harvesting at this frequency region too. 3D gain patterns, shown in Figure 7, depict gain values exceeding 3.8dB at the central frequency of 940MHz. At all frequencies, maximum gain values appear at the broadside direction (perpendicular to the structure's plane) which is an essential attribute for antennas used for rectenna applications.

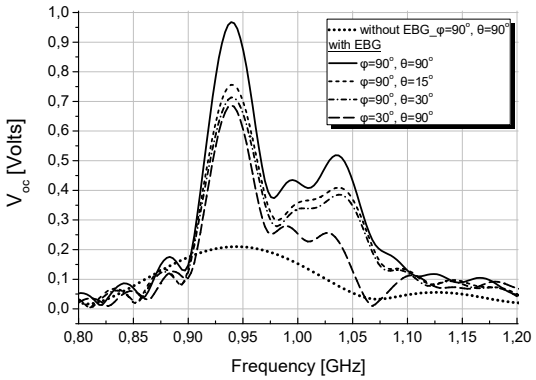

Figure 6: V_{oc} against frequency for the proposed system with and without the EBG for different DoAs (θ,φ)

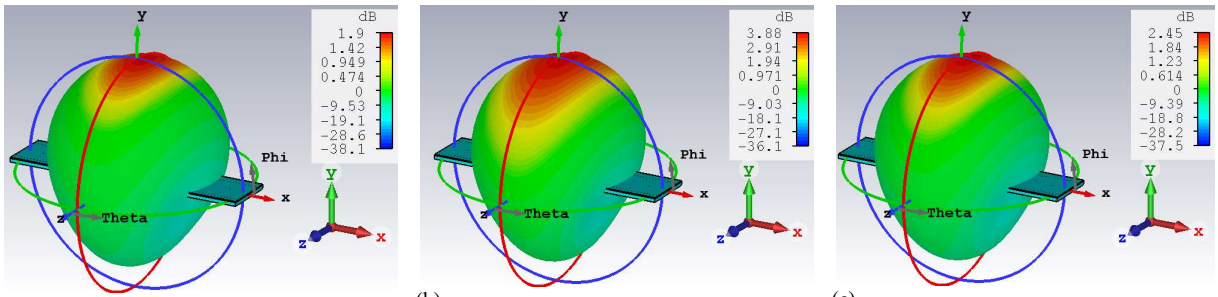

Figure 7: Radiation patterns for the Gain at (a) 920MHz, (b) 940MHz and (c) 960MHz

As previously discussed, the input impedance of the entire antenna is crucial and necessary for the synthesis of MN. The input - output port of the loop antenna (Figure 4a) and the values of the input impedance, Z_{in}, versus frequency were calculated via simulations. The results are depicted in Figure 8.

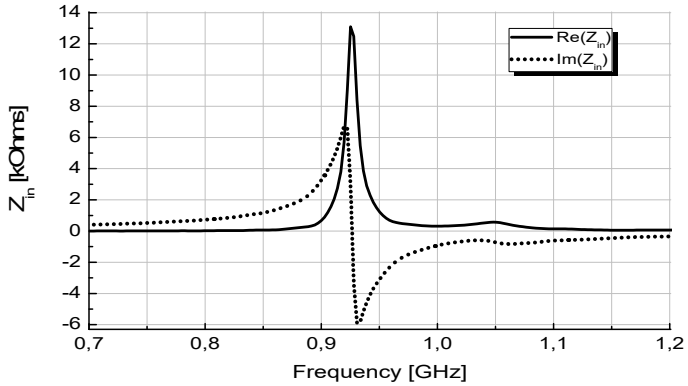

Figure 8: The loop antenna's input impedance versus frequency. Results received via simulation

The available voltage and power at the input of the rectifier, termed as V_{inrec} and P_{inrec} and the resulting DC voltage, V_{DC}, at its output, are proportional to the power of the RF waves incident at the antenna, their DoAs, the frequency and the Matching Network's design. The antenna gain also relies on frequency and DoAs and in turn the respective V_{oc} values. In order to approach the rectenna's performance realistically, namely simulating urban conditions, the aforementioned magnitudes were calculated for a wide range of DoAs. Secondly, a statistical analysis over the DoAs and frequencies in the 940MHz band took place.

The quantities V_{inrec} and P_{inrec} can be estimated, generally, via three ways: a) extract simulated V_{oc} values induced at the antenna's open-circuited input terminals, without the presence on the rectifier and the matching network, for every DoA of the incoming waves and then use these V_{oc} values along with the respective theory of the circuitry of matcher and rectifier b) at first obtain via simulations the antenna's Gain for multiple directions which are homologous to the incoming waves' DoAs, then apply the respective antenna theory to

calculate the power collected by the antenna (Balanis, 2016) and finally estimate the V_{inrec} and P_{inrec} applying the corresponding theory of circuits and c) calculate all magnitudes completely and directly through simulation, integrating all elements in the structure i.e. the antenna, the rectifier and the MN' s elements. The results which follow were extracted via the third way.

To assess the rectenna's ability to scavenge the surrounding radiation power, cases of waves impinging on the antenna from various DoAs were simulated within a conical area ± 45° around the frontal direction (y-axis) of the antenna to emulate urban and suburban scenarios where perpendicular incidence barely occurs. The impinging plane waves were considered circularly polarized (CP) with an amplitude of electric field intensity equal to 1V/m. As previously presented (Figure 6), waves arriving from directions around the frontal area of the antenna yield higher V_{oc} values that may reach 0.97V/m. In all cases, maximum V_{oc} values for all DoAs appeared at 940MHz since it is the central frequency of operation and at which the EBG was designed to resonate.

A rectenna's main metrics, are the DC voltage, V_{DC}, at the output of the rectifier and the power, P_{inrec}, to be transferred at the rectifier. The calculations of both quantities were extracted directly via simulations, as aforementioned. Figure 9, demonstrates, indicatively, V_{DC} values over frequency for various DoAs (θ,φ). Maximum V_{DC} value reached 0.42V at 940MHz since this is the resonant frequency and for direction of arrival of the wave (φ=90°, θ=90°). The majority of the values exceeded 0.25V implying immunity as far as it concerns the reception ability from oblique incidence. Regarding the power available, at the rectifier's input, the corresponding results are presented in Figure 10. The maximum P_{inrec} value recorded was 25.3μW, at 940MHz, and obtained from the previously mentioned DoA. In general, maximum values of V_{DC} and P_{inrec} appear at the central frequency, 940MHz, as expected, and for directions around the perpendicular one, since V_{oc} induced at the loop antenna also exhibits maximum values under these conditions.

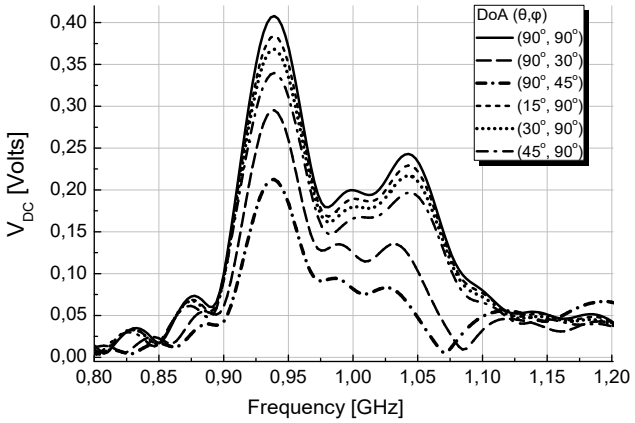

Figure 9: DC Voltage at the rectifier's output against frequency for different DoA (θ,φ)

Having simulated the EBG rectenna for thirteen (13) different combinations of (θ,φ) and for seventeen (17) frequencies in the 940MHz frequency regime, a statistical sample of 221 values for V_{DC} and P_{inrec} were obtained. Respective box plots for these values exhibit interesting results for the capabilities of the proposed hybrid antenna.

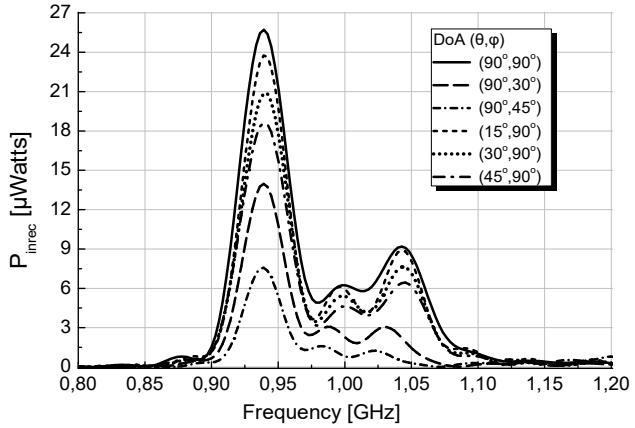

Figure 10: Power available at the rectifier's input against frequency for different DoA (θ,φ)

For V_{DC}, mean value reached 318mV while minimum and maximum values were 142mV and 415mV respectively. Q1 (percentile 25%) was equal to 270mV and Q2 (percentile 75%) to 349mV (Figure 11a). Interquartile (IQR) range for Pin_rec, extends from 10.3μW (percentile 25%) to 19.6μW (percentile 75%), while mean, minimum and maximum values were equal to 14.8μW, 2.03μW and 26.0μW (Figure 11b). As a final criterion for the rectenna's overall performance, the values of the power efficiency, n [%], were calculated. The efficiency was defined as the power P_{inrec} , that reaches at the rectifier's input, over the ambient power captured from the antenna. The power values were calculated, in accordance to the antenna theory, by the simulated values of its Gain, the wavelengths and power of the incident waves [W/m^2], considering electric field intensity of 1V/m. The antenna Gain values were calculated towards all the DoAs used for calculation of V_{DC} and P_{inrec}. Statistical results are shown in Figure 11c. A mean efficiency ~61.5% is obtained while the minimum and maximum values are ~30% and ~83%. The reported efficiency is superior to respective rectenna structures without EBG (Huang, et al., 2020; Rivière, et al., 2020).

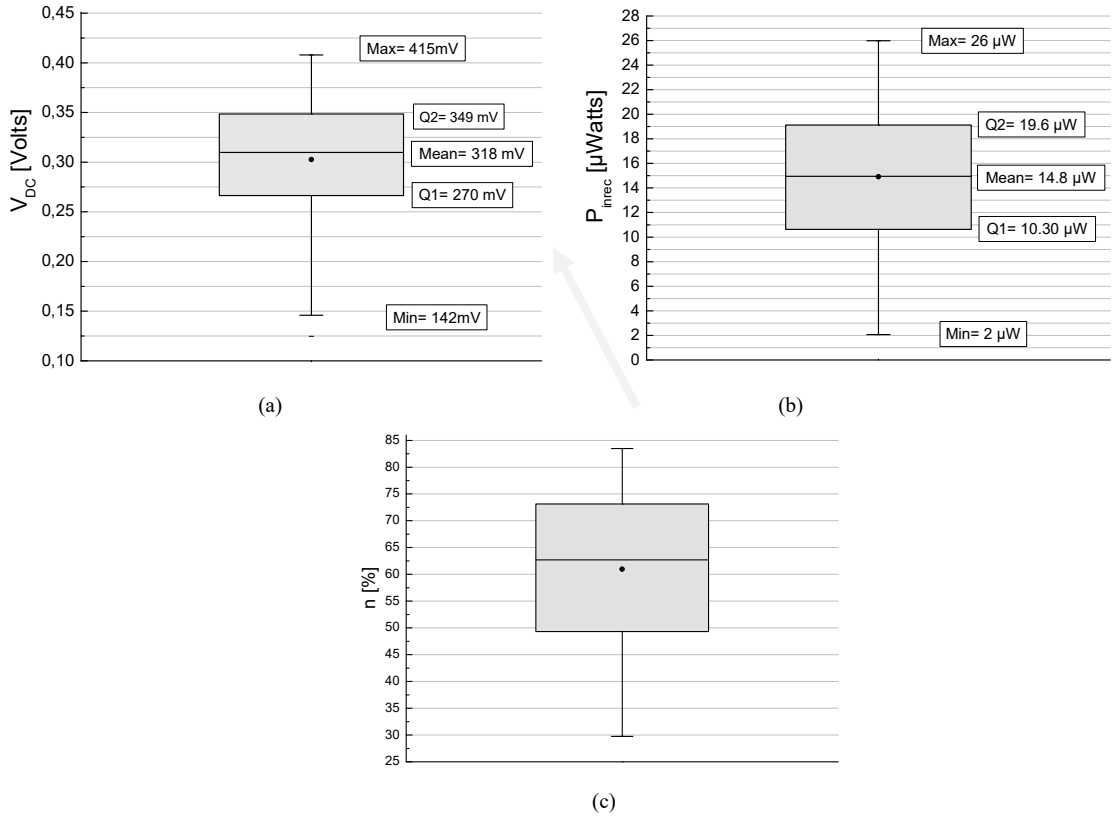

Figure 11: Statistics for V_{DC} , P_{in_rec} and the efficiency n. Box plots over frequencies and DoAs for a) V_{DC} b) $P_{in\_rec.}$ c) Power efficiency n[%]

V. CONCLUSIONS

In this work, a novel rectenna system consisting of a printed loop antenna and an EBG is investigated in terms of its performance at the 940MHz frequency regime, simulating urban environment conditions. The EBG lattice was exploited concerning its ability to exhibit, at its resonance, EM fields of high intensity at the perimeter of its patches in order to enhance the EM energy harvesting of the simple printed loop antenna. The EBG consists of six (6) identical and equally spaced patches integrated in a substrate layer, covered by another dielectric layer and was precisely tuned to resonate at 940MHz enhancing the rectenna's overall performance The proposed antenna can effectively receive electromagnetic waves from a wide range of DoAs and when connected to a full-wave rectifier through a specially designed matching network, it proved to yield satisfactory high DC voltages at the rectifier's output and satisfactory power P_{inrec} at its input.

The total simulated V_{oc} received at the proposed antenna's open circuited terminals was increased fivefold compared to a respective structure lacking the EBG lattice, validating the necessity of the EBG. V_{oc} and Gain amplification are attributed to the high electromotive force in the loop induced by the magnetic field of the EBG structure as the loop antenna is in close proximity to the latter.

Statistical analysis on DC voltage (V_{DC}) and input power at the rectifier (P_{inrec}) demonstrated mean values of 318 mV and 14.8μW respectively, for various DoAs of incoming waves. Moreover, maximum values

obtained for V_{DC} and P_{inrec}, were 415V and 26.1μW while for the 50% of DoAs, V_{DC} values range from 270.15mV to 349.4mV and P_{inrec} values from 10.355μW to 19.675μW.

It is worth noting that the incoming waves' polarization was intentionally chosen to be circular to approach the rectenna's behavior realistically with the expense of obtaining lower V_{DC} and P_{inrec} values at the rectifier as compared to choosing linear polarization which yields higher V_{oc} values.

ACKNOWLEDGMENT

The research has been co-financed by the European Union and Greek national funds through the Operational Program Competitiveness, Entrepreneurship and Innovation, under the call Research-CREATE-INNOVATE (project code: T1EDK-05274).

REFERENCES

[1]. Abdulhameed, M. K., et al. 2019. Radiation control of microstrip patch antenna by using electromagnetic band gap. International Journal of Electronics and Communications (AEÜ), 110:152835, 1-11. https://doi.org/10.1016/j.aeue.2019.152835.

[2]. Abdulhameed, M., Isa, M. S. M., Ibrahim, I. M., Zakaria, Z., Mohsen, M. K., Attiah, M. L., Dinar, A. M. 2020. Side lobe reduction in array antenna by using novel design of EBG. International Journal of Electrical and Computer Engineering, 10:1, 308-315, ISSN: 2088-8708. DOI: 10.11591/ijece.v10i1.

[3]. Assimonis, S. D. and Fusco, V. 2018. RF Energy harvesting with dense rectenna-arrays using electrically small rectennas suitable for IoT 5G embedded sensor nodes. IEEE MTT-S International Microwave Workshop Series on 5G Hardware and System Technologies (IMWS-5G), Dublin, Ireland, 1-3. doi:10.1109/IMWS-5G.2018.8484384.

[4]. Avago Technologies, 2020. Data Sheet HSMS-285x. https://pdf1.alldatasheet.com/datasheetpdf/view/1072262/AVAGO/H SMS-285X.html

[5]. AVX-Advanced Electronic Components, 2020. https://www.avx.com

[6]. Awal, M. R., Jusoh, M., Sabapathy, T., Kamarudin, M. R., Rahim, R. A. 2016. State-of-the-art developments of acoustic energy transfer. International Journal of Antennas and Propagation, Article ID 3072528, 14 pages. https://doi.org/10.1155/2016/3072528.

[7]. Azarbar, A and Ghalibafan, J. 2011. A Compact Low-Permittivity Dual-Layer EBG Structure for Mutual Coupling Reduction. International Journal of Antennas and Propagation, Hindawi Publishing Corporation, 2011, Article ID 237454. doi:10.1155/2011/237454.

[8]. Balanis, C.A. 2016. Antenna Theory: Analysis and Design, 4th ed., John Wiley & Sons: Hoboken, NJ, USA

[9]. Chen, R., Lee, Y. C., Sun, J. S. 2009. Design and experiment of a loop rectenna for RFID wireless power transmission and data communication applications. Progress In Electromagnetics Research Symposium, Beijing, China, March 23–27.

[10]. Divakaran, S. K. and Krishna, D. D. 2019. RF energy harvesting systems: An overview and design issues. International Journal of RF and Microwave Computer-Aided Engineering, 29:1, p.e21633.

[11]. Egashira, S., Nishiyama, E., Toyoda, I. 2020. Experimental study on 2-Element rectenna array using Yagi-Uda antenna. International Symposium on Antennas and Propagation (ISAP), 521-522. doi:10.23919/ISAP47053.2021.9391191.

[12]. Hong, T., Oh, K. M., Lee, H. W., Nam, H., Yun, T., Lee, D.S., Hwang, H., Lee, J. 2010. Novel broadband rectenna using printed monopole antenna and harmonic suppressed stub filter. Microwave and Optical Technology Letters, 52:5, 1194-1197.

[13]. Hou, L., Tan, S., Zhang, Z., Bergmann, N. W. 2018. Thermal energy harvesting WSNs node for temperature monitoring in IIoT. IEEE Access, 6, 35243–35249.

[14]. Huang, J., Yu, S., Kou, N., Ding, Z., Zhang, Z. 2020. Dual-Band rectenna for wireless information and power transmission of WLAN applications. Progress In Electromagnetics Research M, 96, 45-54. doi:10.2528/PIERM20072703.

[15]. Imran, A. I., Elwi, T. A., Salim, A. J. 2021. On the Distortionless of UWB wearable hilbert-shaped metamaterial antenna for low energy applications. Progress In Electromagnetics Research M, 101, 219-239. doi:10.2528/PIERM20113008.

[16]. Jianwei, J., Pang, J., Wang, S., Qiu, Z., Liu, C. 2020. A compact hollowed-out loop rectenna without matching network for wireless sensor applications. International Journal of Rf and Microwave Computer-aided Engineering, 30:20. DOI: 10.1002/mmce.22417.

[17]. Johanson Technology, 2020. https://www.johansontechnology.com

[18]. Kang, E., Lim, T. H., Youn, S., Lee, D. H., Kim, K. B., Choo, H. 2020. Design of a miniaturized printed multi-turn loop antenna for shielding effectiveness measurement. IEEE Access, 8, 54872-54878. doi:10.1109/ACCESS.2020.2980932.

[19]. Khosht, R.M., Feshawy, M. A., Shorbagy, M. A., Farag, M. N., Said, A. E., Hammad, H., Abdel-Hamid, A. T. 2016. A foldable textile-based broadband archimedean spiral rectenna for RF energy harvesting. 2016 16th Mediterranean Microwave Symposium (MMS), 1-4.

[20]. Kildal, P. S., Kishk, A. A., Maci, S. 2005. Special issue on artificial magnetic conductors, soft/hard surfaces, and other complex surfaces. (Guest Editorial), IEEE Transactions on Antennas and Propagation, 53:1, 2-7. DOI:10.1109/TAP.2004.841530.

[21]. Kim, S., et al. 2014. Ambient RF energy-harvesting technologies for self-sustainable standalone wireless sensor platforms. Proceedings of the IEEE, 102:11, 1649-1666. doi: 10.1109/JPROC.2014.2357031.

[22]. Lee, W., Kim, H., Yoon, Y. K. 2020. Metamaterial-inspired dual-function loop antenna for wireless power transfer and wireless communications. 2020 IEEE 70th Electronic Components and Technology Conference (ECTC), Orlando, FL, USA, 1351-1357. doi: 10.1109/ECTC32862.2020.00214.

[23]. Liu, W., Huang, K., Zhou, X., Durrani, S. 2019. Next generation backscatter communication: systems, techniques, and applications. J.Wireless Com. Network, Article 69, https://doi.org/10.1186/s13638-019-1391-7.

[24]. López, A., Onel, L., Alves, H., Souza, D. R., Samuel, M. S., Fernández, G., Evelio, M., Matti, L. 2019. Massive wireless energy transfer: enabling sustainable IoT towards 6G era. https://arxiv.org/abs/1912.05322.

[25]. Mouapi, A., Hakem, N., Delisle, G. Y., Kandil, N. 2015. A novel piezoelectric micro-generator to power wireless sensors networks in vehicles. Proceedings of the 2015 IEEE 15th International Conference on Environment and Electrical Engineering (EEEIC), Rome, Italy, 10–13 June, 1089–1092.

[26]. Mourtzios, C., Ganatsos, T., Siakavara, K. 2014. MEG and correlation characteristics of hybrid dipole — nonuniform EBG antenna systems. The 8th European Conference on Antennas and Propagation (EuCAP 2014), The Hague, Netherlands, 2839-2843. doi: 10.1109/EuCAP.2014.6902418.

[27]. Nguyen, C. V., Nguyen, M. T., Quyen, T. V., Le, A. M., Masaracchia, A., Nguyen, H. T., Nguyen, H. P., Nguyen, L. D., Nguyen, H. T., Nguyen, V. Q. 2020. Hybrid solar-RF energy harvesting systems for electric operated wheelchairs. Electronics, 9:5, 752. 10.3390/electronics9050752.

[28]. Peddakrishna, S. K., Asok, T. D. 2017. Electromagnetic band-gap structured printed antennas: a feature-oriented survey. International Journal of RF and Microwave Computer-Aided Engineering, 27:7. doi.org/10.1002/mmce.21110.
[29]. Pinuela, M., Mitcheson, P. D., Lucyszyn, S. 2013. Ambient RF energy harvesting in urban and semi-urban environment. IEEE Trans. Microw. Theory Tech., 61:7, 2715–2726.
[30]. Pozar, D. M. 2012. Microwave Engineering. 4th ed., John Wiley & Sons: Hoboken, NJ, USA
[31]. Rashmi, P., Shankhwar, A. K., Singh, A. 2021. An improved conversion efficiency of 1.975 to 4.744 GHz rectenna for wireless sensor applications. Progress In Electromagnetics Research C, 109, 217-225, 2021. doi:10.2528/PIERC20121102.
[32]. Rivière, J., Douyère, A., Cazour, J., Alicalapa, F., Lan Sun Luk, J. D. 2016. Co-simulation of a complete rectenna with a circular slot loop antenna in CPW technology. IOP Conference Series: Materials Science and Engineering, 198, IEEE Radio and Antenna Days of the Indian Ocean 10–13 October, Réunion Island, France
[33]. Sandhya Lakshmi, R.,2015. RF Energy Harvesting for Wireless Devices. International Journal of Engineering Research and Development, 11(04), 39- 52. e-ISSN: 2278-067X, p-ISSN: 2278-800X.
[34]. Shen, S., Zhang, Y., Chiu, C. Y., Murch, R. 2019. An ambient RF energy harvesting system where the number of antenna ports is dependent on frequency. IEEE Trans. Microw. Theory Techn., 67:9, 3821-3832.
[35]. Shi, Y., Jing, J., Fan, Y., Yang, L., Wang, M. 2018. Design of a novel compact and efficient rectenna for WiFi energy harvesting. Progress In Electromagnetics Research C, 83, 57–70. doi:10.2528/PIERC18012803.
[36]. Shital, L., Vaishali, D., 2017.Microstrip antenna array with Square EBG Structure. IOSR Journal of Electronics and Communication Engineering (IOSR-JECE) e-ISSN: 2278-2834, p- ISSN: 2278-8735. 12(6), Ver. I, 58-62 DOI: 10.9790/2834-1206015862.
[37]. Sievenpiper, D., Zhang, L., Broas, R. F. J., Alexopoulos, N. G., Yablonovitch, E. 1999. High-impedance electromagnetic surfaces with a forbidden frequency band. IEEE Transactions on Microwave Theory and Techniques, 47:11, 2059-2074. doi: 10.1109/22.798001.
[38]. Song, C., Huang, Y., Carter, P., Zhou, J., Yuan, S., Xu, Q., Kod, M. 2016. A novel six-band dual CP rectenna using improved impedance matching technique for ambient RF energy harvesting. IEEE Transactions on Antennas and Propagation, 64:7, 3160-3171. https://doi.org/10.1109/TAP.2016.2565697.
[39]. Su, S. W. 2011. Printed loop antenna integrated into a compact, outdoor WLAN access point with dual-polarized radiation. Progress In Electromagnetics Research C, 19, 25-35. doi:10.2528/PIERC10102602.
[40]. Wang, M., Yang, L., Shi, Y. 2020. A dual-port microstrip rectenna for wireless energy harvest at LTE band. AEU - International Journal of Electronics and Communications, 126, 153451, ISSN 1434-8411. https://doi.org/10.1016/j.aeue.2020.153451.
[41]. Wu, T., Chen, J., Wu, P.F. 2020. Multi-Mode high-gain antenna array loaded with high impedance surface. IEEE Access, 8, 147070-147076. doi:10.1109/ACCESS.2020.3015758.
[42]. Yala-Ruiz, D. C., Atoche, A., Ruiz-Ibarra, E., Osorio de la Rosa, E., Vázquez Castillo, J. 2019. A self-powered PMFC-based wireless sensor node for smart city applications. Wirel. Commun. Mob. Comput., Article ID:8986302.
[43]. Zeng, M., Andrenko, A. S., Liu, X., Li, Z., Tan, H. 2017. A Compact fractal loop rectenna for RF energy harvesting. IEEE Antennas and Wireless Propagation Letters, 16, 2424-2427. doi:10.1109/LAWP.2017.2722460.
[44]. Zhang, L., Huang, S., Huang, Z. X., Liu, C., Wang, C., Wang, Z., Yu, X., Wu, X. L. 2020. Miniaturized notched ultra-wideband antenna based on EBG electromagnetic bandgap structure. Progress In Electromagnetics Research Letters, 91, 99-107. doi:10.2528/PIERL20041005.
[45]. Zhang, Y., Shen, S., Chiu, C. Y., Murch, R. 2019. Hybrid RF-solar energy harvesting systems utilizing transparent multiport micromeshed antennas. IEEE Transactions on Microwave Theory and Techniques, 67:11, 4534-4546. doi: 10.1109/TMTT.2019.2930507.
[46]. Zhu, J., Hu, Z., Song, C., Yi, N., Yu, Z., Liu, Z., Liu, S., Wang, M., Dexheimer, M. G., Yang, J., Cheng, H. 2021. Stretchable wideband dipole antennas and rectennas for RF energy harvesting. Materials Today Physics, 18, article number:100377, ISSN 2542-5293. https://doi.org/10.1016/j.mtphys.2021.100377.

Christos Mourtzios, et. al. “Synthesis of a printed loop rectenna using metamaterials for effective RF energy harvesting." *International Journal of Engineering Research and Development*, vol. 17(04), 2021, pp 51-62.